An SOC-Based Battery Management System for Microgrids

Zhixin Miao, *Senior Member, IEEE,* Ling Xu, *Student Member, IEEE,* Lingling Fan, *Senior Member, IEEE* and Vahid R. Disfani, *Student Member, IEEE*

***Abstract*—This paper investigates modeling and control of a battery management system used in a microgrid for both grid-connected and autonomous modes. The paper has three salient contributions: 1) An aggregated battery circuit model with the open circuit voltage as a nonlinear function of the state of the charge (SOC) is derived and modeled in PSCAD. 2) Closed-loop feedback control strategies of the battery system are developed for the microgrid under both operation modes. At the grid-connected mode, power control is employed while at the autonomous mode, voltage and frequency control is employed for the battery to act as a synchronous generator by providing voltage and frequency support. 3) An upper level SOC based management system is also developed. Since SOC cannot be directly measured, an estimation scheme is derived based on power and voltage measurements from the battery. The overall management system is demonstrated to be effective by five case studies at different microgrid operation modes.**

***Index Terms*—Battery Model, State of Charge (SOC), Li-Ion battery, Energy Storage Systems (ESS), Battery Management System**

I. Introduction

MICROGRID is an important technology to integrate distributed energy resources, including wind turbines, solar photovoltaic panels and energy storage devices such as battery [1]–[5]. A microgrid can either operate at the grid connected or autonomous modes [6], [7].

At autonomous modes, voltage and frequency should be supported by a microgrid itself, usually through synchronous generators. For a microgrid without synchronous generators, the system voltage and frequency would be difficult to maintain without the support of the ac grid. One solution is to use a voltage source converter (VSC) interfaced energy sources to provide voltage and frequency control [8]. In [8]–[10], battery systems are employed to restore system voltage and frequency quickly (several cycles). In practice, applications of battery storage system for grid frequency regulation have been deployed [11] with the maximum capacity of 20 MW.

At grid-connected modes, VSCs of battery systems can work at power control mode. Depending on the state of charge (SOC) of battery and active power requirement by the microgrid, a battery may operate at either charging or discharging conditions. The VSC connected between the battery and the microgrid regulates power flow only. In [12] and [13], applications of battery energy storage systems in grid power balance at grid-connected modes are demonstrated.

An ideal DC voltage source is assumed for a battery in [6]–[8]. In reality, a battery has operation limits. For example, the SOC cannot be lower than a threshold; the Depth of Discharge (DOD) may affect the life time of a battery [11]. Therefore, there is a need to model a battery accurately and develop control strategies based on the comprehensive battery model with battery status information collected.

Detailed battery models have been developed in the literature. In [14], a battery model is described by partial differential equations. [2] adopted the same model to simulate a wind farm with a Lead-acid battery system. A Li-ion battery has been a suitable choice for high power application due to breakthroughs on materials [11]. Reference [15] describes a detailed Li-ion battery model with parameters and has verified the validity through experiments. Though the battery studied in [15] is for a low voltage level, serial and parallel connections could make a high voltage and high power battery matrix possible, which could be used in power system [16].

The objective of this paper is to develop control strategies for a battery system to improve operation of a microgrid. The control strategies will not only provide system requirements but also take safe operation of a battery into consideration. An aggregated battery model suitable for high power application will be derived base on the cell model presented in [15]. A comprehensive model for a microgrid, with a battery system, an induction machine and passive loads will be built in PSCAD/EMTDC. Control strategies will be developed and verified through simulation studies.

The paper is organized as follows. In Section II, the aggregated battery model is derive. Next, SOC-based battery management system (BMS) and its components will be introduced in Section III. Section IV presents case studies to demonstrate the effectiveness of the BMS. Section V concludes the paper.

II. Battery Model

An accurate electrical battery cell model is represented in [15] for 4.1-V, 850-mAh TCL PL-383562 Li-ion batteries. In this paper, an aggregated model based on the cell model presented in [15] will be developed. Fig 1 illustrates how series and parallel connections of battery cells create battery branches and battery module. Note that a battery module consists of M branches and each branch consists of N cells.

Z. Miao, L. Xu, L. Fan, and V. R. Disfani are with Department of Electrical Engineering at University of South Florida, Tampa, FL (Emails: zmiao@usf.edu; lxu@mail.usf.edu; linglingfan@usf.edu; and vahid@mail.usf.edu).

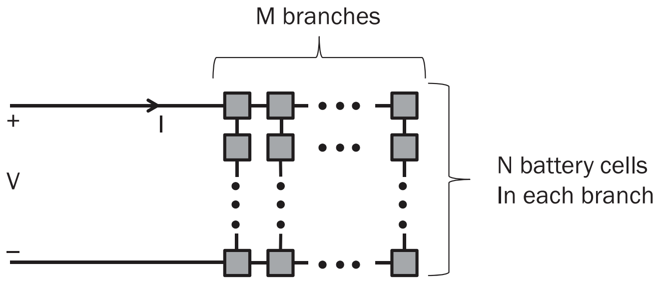

Fig. 1. Aggregation of battery cells to create a battery module.

A. Battery Branch Model

A branch is formed by connecting N battery cells in series together in order to increase the voltage of the battery. Since the current flowing through the battery branch equals to that of the battery cells due to their series connection, it is correct to assume that the left part of the equivalent circuit of battery branch and battery cell are exactly the same. On the right part of equivalent circuit, it is obvious that the branch voltage is N times greater than the voltage of a battery cell, so the value of V_{OC} of the branch is N times greater than that of a battery cell. Moreover, as the resistors and capacitors of the battery cells are connected in series, we can replace them with their equivalent values. Fig. 2 depicts the equivalent circuit describing the model of a battery branch.

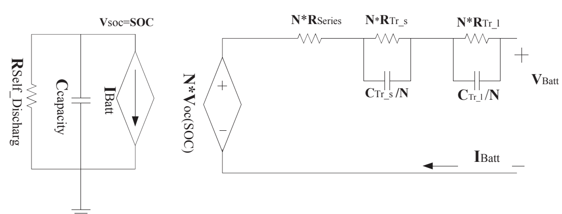

Fig. 2. Equivalent Circuit of a Battery Branch created by N series-connected Battery Cells.

B. Battery Module Model

The next step for aggregation of battery cells to create a battery module is to connect M battery modules in parallel in order to increase the size of battery. In parallel connection of battery branches, the voltage across the battery module is equal to the voltage of branches. On the other hand, the current flowing through the module is M times greater than the current in battery branches and battery cells. Therefore, the Current-Controlled Current Source located in left part of the equivalent circuit must be modified. Due to parallel connection of branches to create battery module, the values of resistors and capacitors are changed compared to those in battery branch equivalent circuit. All these modifications are illustrated in 3.

The model developed in this paper for the battery module aggregated from the battery cells has been simulated and tested via PSCAD/EMTDC and the results have demonstrated the accuracy of model represented.

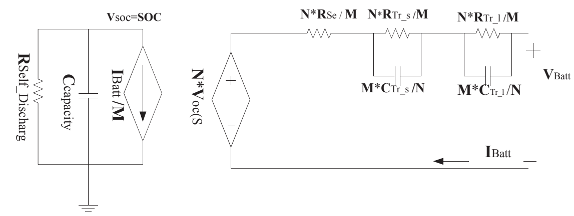

Fig. 3. Equivalent Circuit of a Battery Module containing M parallel Battery Branches.

III. SOC-based Battery Management System

The management system proposed in this paper is a hierarchical control system containing three modules named SOC Computation Module, Battery Mode Identification System (BMIS), and Closed-Loop Feedback Controller (CLFC). The function of BMIS is to determine the appropriate reference values as well as the mode in which the battery be operated considering SOC. Fig. 4 shows the configuration of proposed battery management system. The BMS receives power order and microgrid connection status from the upper operation center. The BMS also receives measurements from the battery to compute SOC. SOC is passed to BMIS to decide if limits are reached and which action should be taken. The BMIS then passes the decision making to the closed-loop feedback control system which generates PWM gate signals to the converters.

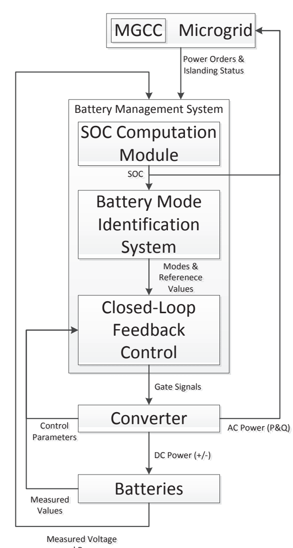

Fig. 4. Proposed BMS Configuration

A. SOC Computation Module

SOC is a measure of the amount of charge stored in a battery, which can be expressed as the percentage of the capacity of the battery and shows energy is left in an energy storage system. The responsibility of SOC computation module is to obtain the SOC based on the battery measurements. This signal is used by BMS to decide accurately about the operation modes and reference signals. BMS also frequently sends the signal of SOC to Microgrid Control Center (MGCC) or in response to its inquiry to inform it how much energy is already stored in the battery, which enables MGCC to use this signal in its optimization procedures. An SOC computation method using coulomb counting technique is employed by the BMS. Since the charge stored in a battery is integration of the current injected to the battery, we have:

$$Q(t) = Q(t-1) + \Delta Q(t) \tag{1}$$

where

$$\Delta Q(t) = I_B(t)\Delta t = \frac{P_B(t)}{V_{DC}(t)}\Delta t \tag{2}$$

where $Q_B(t)$, $I_B(t)$, $P_B(t)$ and V_{DC} are the charge stored in, current and power injected to, and dc-link voltage of the battery module, respectively.

SOC can be derived by (3) where $Size_B$ identifies battery size in kWh.

$$SOC(t) = SOC(t-1) + \frac{1}{3.6}\frac{1}{Size_B}\frac{P_B(t)}{V_{DC}(t)}\Delta t \tag{3}$$

B. Battery Mode Identification System

Based on SOC and the islanding status of microgrid, BMIS determines the appropriate battery operation mode. Three modes of operation are defined in the BMS proposed in this paper; a) grid-connected discharging mode or PQ control mode, b) grid-connected charging mode, and c) islanding mode or VF control mode. As shown in Fig. 5, in case that the microgrid is connected to the main grid, MGCC expects the battery to follow the power orders dictated to BMS. BMS follows the power order as long as the SOC is greater than its minimum limit. Otherwise, the battery must be charged via injecting a predetermined power to the battery and its mode changes to the charging mode until the SOC meets its maximum limit. In order to make sure that SOC never meets 100%, a function is applied to reduce the power injected to the battery when SOC is more than 90% (4); otherwise charging current is equal to its predetermined value.

$$I_{charging} = I_{predefined}\frac{100 - SOC(\%)}{100} \tag{4}$$

As sudden changes in the current injected to the battery likely cause damages to the battery, increasing and decreasing ramp rates are considered to determine the reference values. After the battery gets charged, the battery will go back to discharging mode. On the other hand, when the microgrid is disconnected from the main grid (islanding mode), microgrid management expects the battery to participate in voltage and frequency regulation process. In this case, BMS changes the operation mode of the battery to islanding mode as long as the SOC does not exceed its limits. Fig. 5 also illustrates how BMS works when the microgrid is in islanding mode. As soon as the microgrid connects again to the main grid, BMS changes the battery control mode to discharging or charging mode according to the value of SOC.

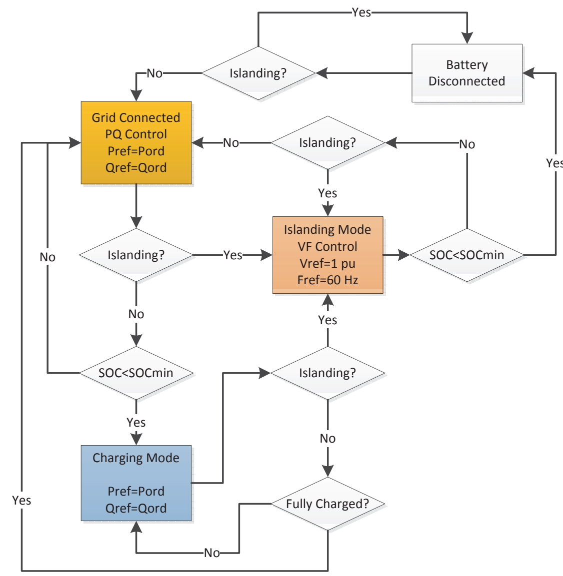

Fig. 5. Functions of Battery Mode Identification System.

C. Closed Loop Feedback Controller (CLFC)

The main objective of the Closed Loop Feedback Controller is to control VSC in order to achieve the goals defined by BMIS. Two different control systems realize microgrid expectations: power control and voltage-frequency control loops. According to BMIS output, CLFC enables either power control loop or voltage-frequency control loop.

1) Power Control Loop: The power control loop gets enabled when the battery control is in grid-connected or charging mode and its duty is to regulate the active and reactive power output from the battery/converter to the microgrid. The CLFC proposed is also capable to regulate dc- and ac-link voltages. Fig. 6 depicts the power control loop with the capability of switching to ac- and dc- link voltage regulating mode. Moreover, to realize the control loops a decoupled d-q direct current control strategy developed in [17], [18] is utilized.

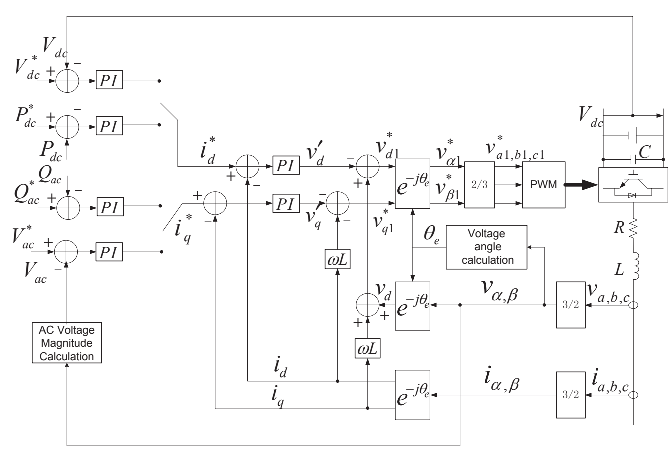

Fig. 6. BMS Power Control Loop.

Variables in the abc system in the above circuits can be transformed into a synchronous reference frame. The voltage and current relationship is shown in (5), where ω_s is the angular frequency of AC system, v_d, v_q, v_{d1}, and v_{q1} represent the d and q components of the point of common coupling (PCC) voltage (V_a, V_b, V_c)and VSC output voltage(V_{a1}, V_{b1}, V_{c1}), respectively, and i_d and i_q represent the d and q components of the current flowing between the AC system and the VSC.

$$\begin{cases} v_{d1} = -(Ri_d + L\frac{di_d}{dt}) + \omega_s L i_q + v_d \\ v_{q1} = -(Ri_q + L\frac{di_q}{dt}) - \omega_s L i_d \end{cases} \quad (5)$$

DC voltage control is based on the balance of active power flow between the battery and the main grid as shown in (6). Apparently, the DC voltage can be regulated by the d axis current through a PI controller.

$$v_{dc}(C\frac{dv_{dc}}{dt} + i_{dc2}) = v_d i_d \rightarrow \frac{v_{dc}}{dt} = \frac{v_d i_d}{v_{dc} C} - \frac{i_{dc2}}{C} \quad (6)$$

2) Voltage and Frequency Control Loop: The voltage-frequency control loop, as illustrated in Fig. 7, is enabled in the mode of islanding and regulated the AC Voltage and frequency of Point of Common Coupling (PCC) on their nominal values since there is no synchronous generator to do so. Despite the fact that the basic control principles used in this paper are generally based on the decoupled current control represented in [7], [19], (5) can be rewritten as (7) in steady-state study of the system where the resistance R is neglected [9], [10]:

$$\begin{cases} V_{d1} = \omega_s L I_q + V_d \\ V_{q1} = -\omega_s L I_d \end{cases} \quad (7)$$

PI controllers can be used to control the d and q axis components of the PCC voltage respectively. Fig. 7 depicts the frequency-voltage control loop. The PCC three-phase voltage is measured and transformed into a $d-q$ reference frame (v_d and v_q). Three-phase current flowing between the loads and the inverter is measured and transformed to i_d and i_q. With the comparisons of the dq voltages to their respective references, the resulting errors are sent to the PI controllers to generate the required output voltage of the VSC.

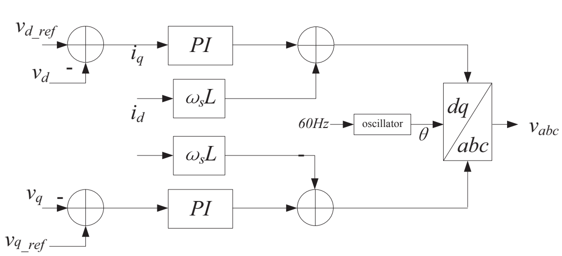

Fig. 7. BMS Voltage and Frequency Control Loop.

The frequency of the AC voltage which supplies passive loads is also controlled by the VSC. An internal oscillator is used to generate the angle θ, which is used as the input of dq to abc transformation and ensures the frequency of output voltage is kept at 60 Hz if PWM scheme applied [20].

IV. Case Study

In order to investigate the responses of the behavior of Battery Management System, five case studies are conducted through PSCAD/EMTDC. The first two cases are designed to make sure BMIS is capable to identify the most appropriate mode of operation as well as accurate signal references while the battery is fully discharged and completely charged, respectively. In the third case study the microgrid is disconnected from the main grid. Battery is expected to be able to maintain the voltage and frequency during islanding mode even if the demand or generation of the power network changes. The forth case study is conducted to study the capability of the BMS during the islanding mode while microgrid demand and/or generation varies. The fifth study is also designated to demonstrate how BMS operates when the battery gets completely discharged during islanding mode.

A. System Topology

A microgrid consisting of a 1-MW bio-diesel machine connected to a 210-kWh battery module is considered as shown in Fig. 8 with the power system parameters listed in Table I in details. The battery module is an aggregation of 60,000 pieces of 4.1-V, 850-mAh TCL PL-383562 Li-ion battery cells introduced in [15] and its characteristics are presented in Table II. The parameters corresponding to the induction generator is also shown in Table III. The microgrid is connected to a strong AC grid via a 69/13.8 kV transformer. A 13.8 kV distribution line based on the IEEE Standard 399-1997 [21] is also included in the model.

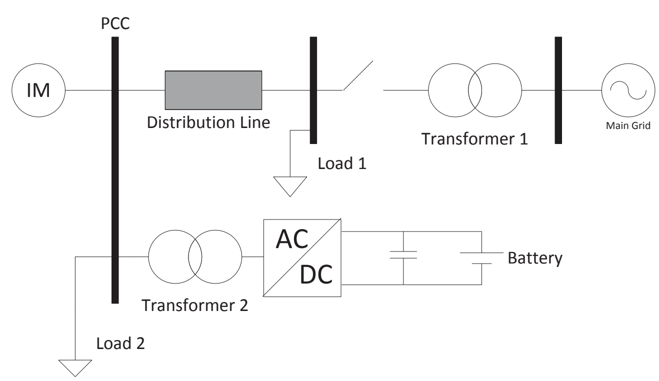

Fig. 8. A microgrid with a battery system.

TABLE I
POWER SYSTEM PARAMETERS

Quantity	Value
AC grid voltage	69kV (L-L RMS)
Transformer 1	13.8kV/69kV, 2MVA, leakage 8%pu
Transformer 2	13.8kV/3.3kV, 1MVA, leakage 10%pu
Load 1	550kW+550kVar at 13.8kV
Load 2	500kW+350kVar at 13.8kV
Distribution line	1187ft, (0.052+j0.0436)ohm

TABLE II
BATTERY CHARACTERISTICS

Quantity	Value
Size	210 kWh
Rated DC Voltage	8.2 kV
Number of Cells in each Branch (M)	2000
Number of Branches (N)	30
Maximum Charging power	840 kW
Increasing Ramp Rate	210 kW/s
Decreasing Ramp Rate	210 kW/s
Full Charge SOC	95%
Full Discharge SOC	5%

TABLE III
INDUCTION MACHINE PARAMETERS

Quantity	Value
Rated RMS phase voltage	5kV
Rated RMS phase current	66.6A
Base angular frequency	60Hz
Stator resistance	0.066pu
First cage resistance	0.298pu
Second cage resistance	0.018pu
Stator unsaturated leakage reactance	0.046pu
Unsaturated magnetizing reactance	3.86pu
Rotor unsaturated mutual reactance	0.122pu
Second cage unsaturated reactance	0.105pu
Polar moment of inertia	1.0s
Mechanical damping	0.0001pu

B. Grid-Connected Mode

In order to evaluate the capability of the BMS in identifying operation modes, two case studies are designed. In these case studies, the battery is ordered to deliver active and reactive power as much as 500 kW and 1 MVar to the microgrid, respectively.

1) Case Study 1- Discharging to Charging: According to the Fig 9, the simulation starts when the SOC of the battery is 13%. SOC meets its minimum limit (5%) at $t = 25.53\ sec$. Consequently, BMIS turns the operation mode from discharging mode to charging mode in order to prevent the battery against Depth of Discharge damages. BMIS also changes the operation mode from discharging mode to charging mode and the active power reference toward predefined charging power (840 kW) respect to the decreasing ramp rate (210 kW/s). After 7 seconds, the reference power becomes constant and the battery absorbs 840 kW active power from the microgrid. An increase in SOC demonstrates that the battery is getting charged. Fig 9 also illustrates that the simulation results V_{soc} exactly matches the computed SOC. The reactive power output of the battery is regulated on the ordered value (1 MVar) and the DC power output follows the variations of AC active power delivered to the microgrid. Fig.10 presents the output current and voltage of the battery, the PCC voltage and the dq-axis currents from the converter.

2) Case Study 2: In this case study, transition from the charging mode to the discharging mode is examined. Fig. 11 presents the simulation results. At the starting time, the SOC is equal to 90.18%. After 44.72 seconds, as soon as the battery charge exceeds 95% of its full capacity, BMIS changes the

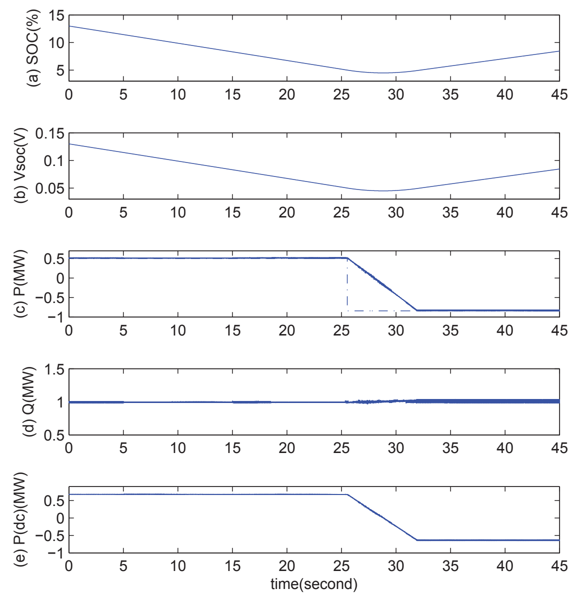

Fig. 9. Case Study 1: (a) SOC, (b) V_{soc}, (c) actual (solid) and reference (dashed) active power delivered to microgrid, (d) reactive power delivered to microgrid, (e) battery DC power output.

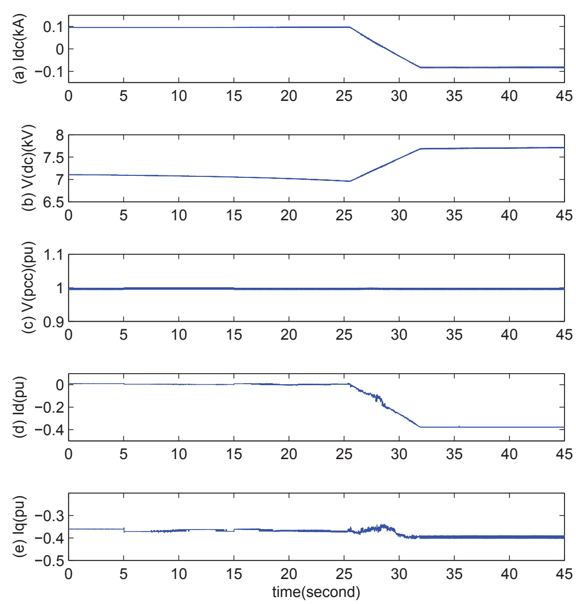

Fig. 10. Case Study 1: (a) battery DC Current, (b) DC Voltage Link, (c) PCC AC Voltage, (d) current d-axis, (e) current q-axis.

operation mode to discharging mode. It also changes the active power order by applying a ramp until it reaches 500 kW after 4 seconds. The CLFC completely follows the power order produced by BMIS, and keeps the reactive power output at 1 MVar.

C. Autonomous Mode

In the next three case studies, the capabilities of the BMS is examined in islanding mode. When the microgrid is disconnected from the main grid, BMIS is expected to change the battery operation mode to islanding mode in order for the

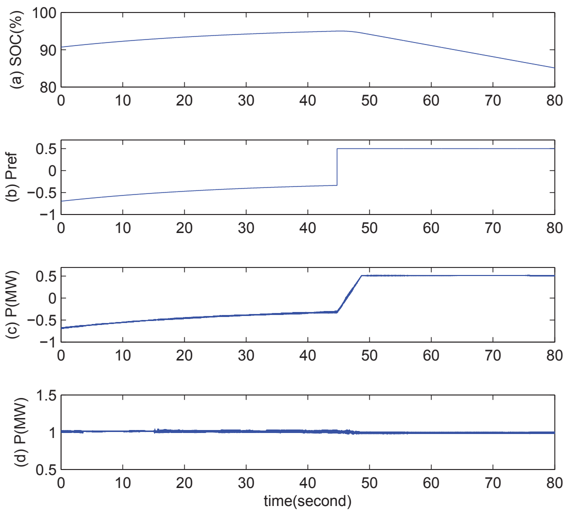

Fig. 11. Case Study 2: (a) SOC, (b) power order, (c) active power delivered to microgrid, (d) reactive power delivered to microgrid.

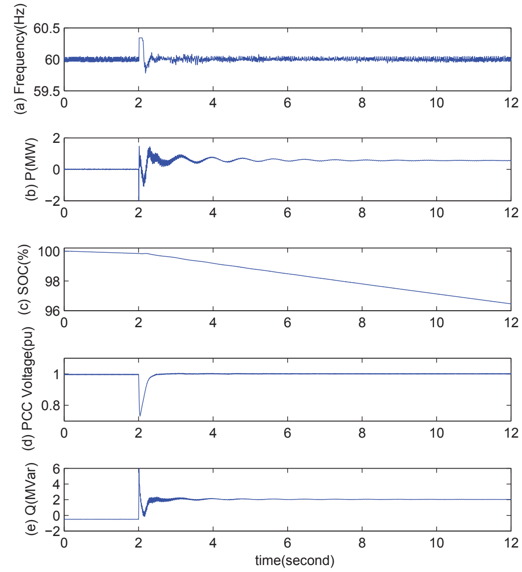

Fig. 12. Case Study 3: Islanding transient: (a) microgrid frequency, (b) active power output of the battery, (c) SOC, (d) AC voltage of PCC, (e) reactive power output of the battery.

CLFC to regulate frequency and AC voltage of the microgrid. BMS is also expected to provide a smooth transition from the grid connected mode to the islanding mode.

1) Case Study 3: In this case study, the microgrid is disconnected from the main grid. The battery is almost completely charged. Transients are observed during the transition period. Fig. 12 illustrates how the microgrid frequency is regulated back to 60 Hz within less than one second. The mechanical torque of the induction generator is fixed and it is under speed control. Therefore, the battery is required to provide power balance for the isolated system. It is shown that the battery increases its output power from 0 kW to 600 kW. The PCC voltage experiences a 0.25-pu drop once the islanding happens according to Fig. 12. Afterward, battery operation adjust the AC voltage to 1 pu in less than one second by injecting 2 MW reactive power to the microgrid. Fig. 13 presents the behavior of the induction generator. The mechanical speed comes back to 1.013 pu within 5 seconds while the torque takes 10 seconds to settle back to -0.8 pu. Note there is no change in steady-state power output from the induction generator.

2) Case Study 4: This case study examines how resilient the battery-integrated microgrid is to respond a loss in generation or demand during islanding operation. Load 1 which absorbs active and reactive powers equal to 550 kW and 550 kVar is disconnected from the microgrid at 30th second of simulation and reconnects after 10 seconds. Fig. 14 presents the voltage and frequency of the microgrid during these events and demonstrates that BMS is capable to balance power in a grid using voltage/frequency control. As expected, the active and reactive power outputs of the battery reduce by approximately 600 kW and 600 kVar to adjust the frequency and AC voltage.

3) Case Study 5: In this case study, it is assumed that the islanding operation of the battery has taken such a long time that the SOC is reaching its minimum limit. In this situation the BMS is expected to disconnect the battery from the microgrid to prevent the battery from serious DOD damages. The simulation starts from SOC equal to 5.9% which meets

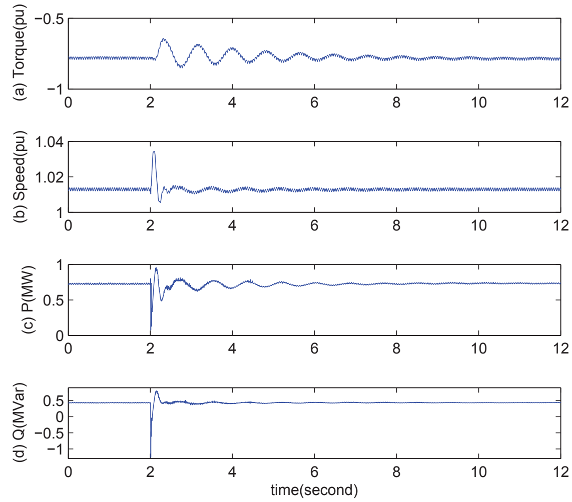

Fig. 13. Case Study 3: Induction generator behavior during the islanding transient: (a) mechanical torque, (b) mechanical speed, (c) active power output of the IG, (d) reactive power output of the IG

its minimum limit after 2.5 seconds. At this point, the battery is disconnected from the microgrid and its active and reactive power changes to zero. As illustrated in Fig. 15, since there is no source to regulate the voltage and frequency of the microgrid, the voltage collapses. Fig. 16 demonstrates that the mechanical torque of induction generator as well as its active and reactive power fall down to zero after some fluctuations due to dynamic characteristics of the induction machine.

V. Conclusion

In order to increase the reliability of a microgrid, it is beneficial to use Energy Storage Systems. Batteries, as the most common types of ESS, must be controlled by a smart

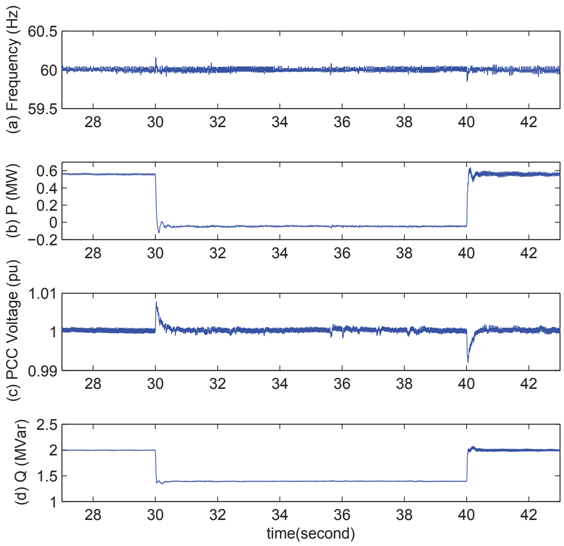

Fig. 14. Case Study 4: Load loss in the islanding mode: (a) microgrid frequency, (b) active power output of battery, (c) AC voltage of PCC, (d) reactive power output of battery.

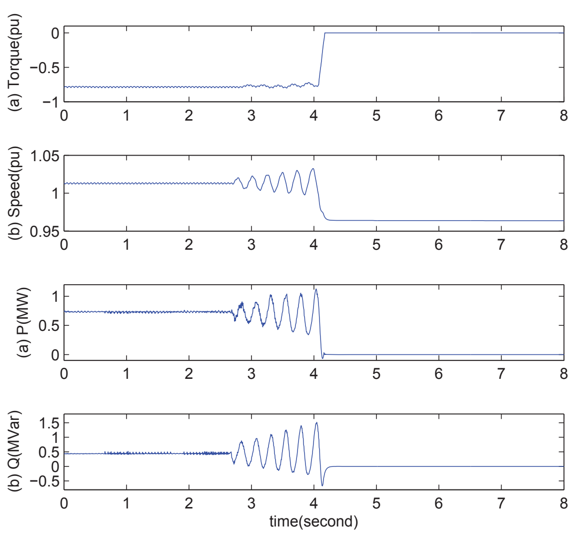

Fig. 15. Case Study 5: Minimum SOC limit reached in the islanding mode: (a) SOC, (b) microgrid frequency, (c) active power output of battery, (d) battery switch status, (e) AC voltage of PCC, (f) reactive power output of battery.

management system. In this paper, an SOC-based Battery Management System (BMS) has been proposed to control the battery considering the islanding status of the microgrid as well as the instantaneous amount of charge stored in the batteries. Three modes of operation were defined for the battery to be operated. A detailed circuit-based aggregated battery model suitable for high power application is developed in this paper to test the BMS. The functionalities of the BMS proposed in this paper are tested through case studies in PSCAD/EMTDC and the dynamic behavior of the microgrid and its components are examined. The simulation results demonstrate the effectiveness of the control strategies through the SOC-based Battery Management System.

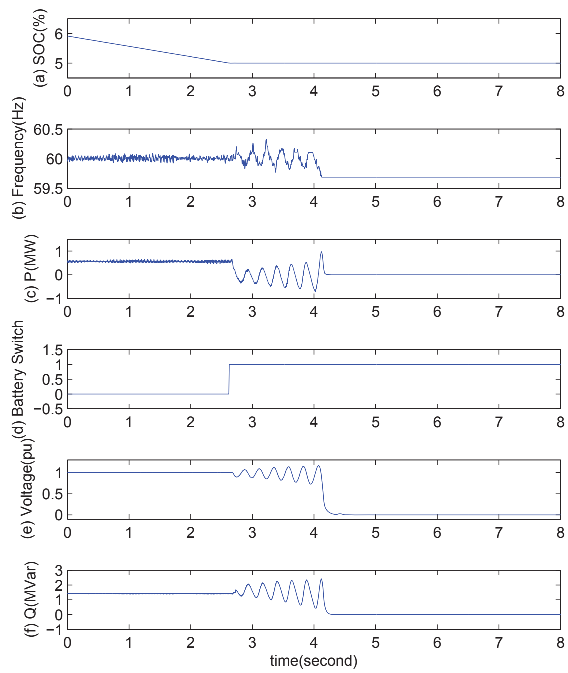

Fig. 16. Case 5: Minimum SOC limit reached in the islanding mode. Induction generator behavior: (a) mechanical torque, (b) mechanical speed, (c) active power output, (d) reactive power output.

Appendix

TABLE IV
PI Controller Parameters of Fig. 6

	Kp	Ki
P control loop	2	10
Q control loop	2	10
DC voltage control loop	1	20
AC voltage control loop	1	20
Id control loop	1.5	100
Iq control loop	1.5	100

TABLE V
PI Controller Parameters of Fig. 7

	Kp	Ki
Vd control loop	3	2
Vq control loop	3	10

References

[1] F. Peng, Y. W. Li, and L. Tolbert, “Control and protection of power electronics interfaced distributed generation systems in a customer-driven microgrid,” in *IEEE Power Energy Society General Meeting*, Jul. 2009, pp. 1 –8.
[2] S. Teleke, M. Baran, A. Huang, S. Bhattacharya, and L. Anderson, “Control strategies for battery energy storage for wind farm dispatching,” *IEEE Trans. Energy Convers.*, vol. 24, no. 3, pp. 725 –732, Sep. 2009.
[3] J.-Y. Kim, J.-H. Jeon, S.-K. Kim, C. Cho, J. Park, H.-M. Kim, and K.-Y. Nam, “Cooperative control strategy of energy storage system and microsources for stabilizing the microgrid during islanded operation,” *IEEE Trans. Power Electron.*, vol. 25, no. 12, pp. 3037 –3048, Dec. 2010.
[4] N. Hatziargyriou, H. Asano, R. Iravani, and C. Marnay, *IEEE Power Energy Mag.*
[5] N. Hatziargyriou, “microgrids [guest editorial],” *Power and Energy Magazine, IEEE*, vol. 6, no. 3, pp. 26 –29, may-june 2008.

[6] C. Smallwood, "Distributed generation in autonomous and nonautonomous micro grids," in *IEEE Rural Electric Power Conference*, 2002, pp. $D1$ –$D1\_6$.

[7] F. Katiraei, M. Iravani, and P. Lehn, "Micro-grid autonomous operation during and subsequent to islanding process," *IEEE Trans. Power Del.*, vol. 20, no. 1, pp. 248 – 257, Jan. 2005.

[8] H. Karimi, H. Nikkhajoei, and R. Iravani, "Control of an electronically-coupled distributed resource unit subsequent to an islanding event," *IEEE Trans. Power Del.*, vol. 23, no. 1, pp. 493 –501, Jan. 2008.

[9] G. Li, M. Yin, M. Zhou, and C. Zhao, "Modeling of VSC-HVDC and control strategies for supplying both active and passive systems," in *IEEE Power Engineering Society General Meeting*, 2006.

[10] H. Chen, "Research on the control strategy of VSC based HVDC system supplying passive network," in *IEEE Power Energy Society General Meeting*, Jul. 2009, pp. 1 –4.

[11] G. L. Soloveichik, "Battery technologies for large-scale stationary energy storage," *Annual Review of Chemical and Biomolecular Engineering*, vol. 2, no. 1, pp. 503–527, 2011.

[12] M. Bragard, N. Soltau, S. Thomas, and R. De Doncker, "The balance of renewable sources and user demands in grids: Power electronics for modular battery energy storage systems," *IEEE Trans. Power Electron.*, vol. 25, no. 12, pp. 3049 –3056, Dec. 2010.

[13] S. Vazquez, S. Lukic, E. Galvan, L. Franquelo, and J. Carrasco, "Energy storage systems for transport and grid applications," *IEEE Trans. Ind. Electron.*, vol. 57, no. 12, pp. 3881 –3895, Dec. 2010.

[14] M. Ceraolo, "New dynamical models of lead-acid batteries," *IEEE Trans. Power Syst.*, vol. 15, no. 4, pp. 1184 –1190, Nov. 2000.

[15] M. Chen and G. Rincon-Mora, "Accurate electrical battery model capable of predicting runtime and i-v performance," *IEEE Trans. Energy Convers.*, vol. 21, no. 2, pp. 504 – 511, Jun. 2006.

[16] J. Dogger, B. Roossien, and F. Nieuwenhout, "Characterization of li-ion batteries for intelligent management of distributed grid-connected storage," *IEEE Trans. Energy Convers.*, vol. 26, no. 1, pp. 256 –263, Mar. 2011.

[17] C. Schauder and H. Mehta, "Vector analysis and control of advanced static var compensators," *IEE Proceedings Gen., Trans. and Dist.*, vol. 140, no. 4, pp. 299 –306, Jul. 1993.

[18] R. Pena, J. Clare, and G. Asher, "Doubly fed induction generator using back-to-back pwm converters and its application to variable-speed wind-energy generation," *Electric Power Applications, IEE Proceedings -*, vol. 143, no. 3, pp. 231 –241, may 1996.

[19] P. Piagi and R. Lasseter, "Autonomous control of microgrids," in *IEEE Power Engineering Society General Meeting*, 2006.

[20] N. Mohan, T. M. Undeland, and W. P. Robbins, *Power Electronics: Converters, Applications, and Design, 3rd Ed.* Wiley, 2002.

[21] "IEEE recommended practice for industrial and commercial power systems analysis," *IEEE Std 399-1997*, p. I, 1998.

Zhixin Miao S'00-M'03-SM'09) received the B.S.E.E. degree from the Huazhong University of Science and Technology at Wuhan China in 1992, the M.S.E.E. degree from the Graduate School, Nanjing Automation Research Institute at Nanjing China in 1997, and the Ph.D. degree in electrical engineering from West Virginia University, Morgantown, in 2002.

Currently, he is with the University of South Florida (USF), Tampa. Prior to joining USF in 2009, he was with the Transmission Asset Management Department with Midwest ISO, St. Paul, MN, from 2002 to 2009. His research interests include power system stability, microgrid, and renewable energy.

Ling Xu received the B.S. degree from Huazhong University of Science and Technology, Wuhan, China, in 2007, the M.S. degree from University of Alabama in 2009.

Currently, he is pursuing a Ph.D. degree at University of South Florida, Tampa, FL. His research interests include power electronic control in power systems, modeling and simulation of renewable energy system.

Lingling Fan (SM'08) received the B.S. and M.S. degrees in electrical engineering from Southeast University, Nanjing, China, in 1994 and 1997, respectively, and the Ph.D. degree in electrical engineering from the University of West Virginia, Morgantown, in 2001.

She is an Assistant Professor at the University of South Florida, Tampa FL since 2009. She was a Senior Engineer in the Transmission Asset Management Department in Midwest ISO, St. Paul,MN (20012007) and an Assistant Professor at North Dakota State University (20072009). Her research interests include control and optimization with applications in wind energy systems, HVDC systems and Phasor Measurement Unit based system identification.

Vahid R. Disfani received his B.S. degree from Amirkabir University of Technology, Tehran, Iran, in 2006, and his M.S. degree from Sharif University of Technology, Tehran, Iran, in 2008.

Currently, he is pursuing a Ph.D. degree at University of South Florida, Tampa, FL. His research interests include Smart Grid, integration of renewable energy resources to microgrids, and electricity markets.